PCCP

RSC Publishing

COMMUNICATION

View Article Online
View Journal | View Issue

Compositional-asymmetry influenced non-linear optical processes of plasmonic nanoparticle dimers†

Cite this: *Phys. Chem. Chem. Phys.*, 2013, **15**, 8031

Received 24th September 2012,
Accepted 7th March 2013

DOI: 10.1039/c3cp43349h

www.rsc.org/pccp

Anke Horneber,[a] Anne-Laure Baudrion,[b] Pierre-Michel Adam,[b] Alfred J. Meixner*[a] and Dai Zhang*[a]

The influences of compositional asymmetry on the two-photon photoluminescence and the second harmonic generation processes in weakly coupled plasmonic dimers were addressed. Au–Au homodimer and Au–Ag heterodimer arrays produced using electron-beam lithography were investigated using confocal nonlinear optical imaging and spectroscopy. Compared to the Au–Au homodimers, the Au–Ag dimers showed slightly broadened two-photon photoluminescence near the *X* symmetry point at the first Brillouin zone of Au, whilst that from the *L* symmetry point stayed the same. Additionally, weakly coupled Au–Ag heterodimers generated strong second harmonic signals which were invisible in the Au–Au homodimers. The observations highlighted the importance of compositional asymmetry in the non-linear optical studies of plasmonic dimers.

Nanostructured metallic materials with sub-wavelength dimensions exhibit usually strong plasmon resonances, which are the essential, dominating factors of their optical properties. Governed by the lightning rod effect and localized surface plasmon resonances (SPR), linear optical properties of metallic nano-antennas have been widely investigated. So far nano-antennas with different geometries have been reported, from single particles like Au spheres[1–4] and nanorods[5–7] to bowtie antennas[8,9] and dimers[10] or the even more complicated Yagi–Uda nano-antennas.[11]

Among them, dimers consisting of two Au nano-spheres with a small gap in between are very commonly investigated. They are known to exhibit a strong near field inside the extremely small gap between the two plasmonically coupled single nanoobjects.[12,13]

To understand how the plasmonic behaviour of individual nanoparticles influences the assembly optical properties of the dimers, models of plasmon coupling between the single particles were viewed to be analogous to molecular hybridization.[14] The plasmon modes of two interacting metal nanoparticles hybridize either in-phase or out-of-phase, forming 'bonding mode' or 'antibonding mode'. Such a model is inevitably influenced by the local density of states, the relative orientations, and the distances between the single nanoparticles in the dimer. Sheikholeslami *et al.* have reported that size-asymmetry and compositional-asymmetry had dramatic influences on the optical resonances of nanoparticle dimers.[15] Based on the gap-field generated by the plasmonic coupling, nonlinear effects like second harmonic generation (SHG), two photon photoluminescence (2PPL),[16] and four-wave-mixing (4WM)[17] were recently investigated. This type of structure has even been studied as a nonlinear photon source for imaging.[18]

Though both are due to the second-order effect, 2PPL and SHG require different preconditions. Compared to the 2PPL process which intrinsically relies on the high optical field, SHG additionally requires materials with high second order susceptibility and symmetry breaking.[19] Such selection rules have to be considered in addition to the 'plasmonic molecular hybridization' model, in order to understand the SHG and the 2PPL efficiencies in metallic dimers. Therefore, we chose arrays of Au–Au homodimers and Au–Ag heterodimers as our experimental systems to study the influences of composition on the non-linear properties of dimer structures. Especially the 2PPL and the SHG signals were compared and analysed.

The sample was prepared using two successive standard e-beam lithography processes. The shape of the Au nanoparticles was e-beam-insolated on a PMMA-coated-glass substrate. Alignment markers were insolated at the same time. After the development, a 50 nm-thick Au layer was evaporated on top of the substrate and the dissolution of the PMMA resist (lift-off) revealed the Au nanoparticles and the markers. After another PMMA coating, the alignment markers were used to insolate the shape of the Ag nanoparticles in the close vicinity of the Au ones. The end of the process (development, Ag evaporation and lift-off) was repeated to obtain Au–Ag heterodimers.

[a] *Institute of Physical Chemistry, Eberhard Karls University Tübingen, Auf der Morgenstelle 15, Tübingen, Germany. E-mail: alfred.meixner@uni-tuebingen.de, dai.zhang@uni-tuebingen.de; Fax: +49 7071 29 5490; Tel: +49 7071 29 77639*

[b] *Laboratoire de Nanotechnologie et d'Instrumentation Optique, Institut Charles Delaunay – UMR CNRS 6279, Université de technologie de Troyes, 12 rue Marie Curie, CS 42060, 10004 Troyes Cedex, France. E-mail: baudrion@utt.fr, pierre_michel.adam@utt.fr; Fax: +33 325718456; Tel: +33 325 718561*

† This paper was submitted as part of a collection of the optical studies of single metal nanoparticles.

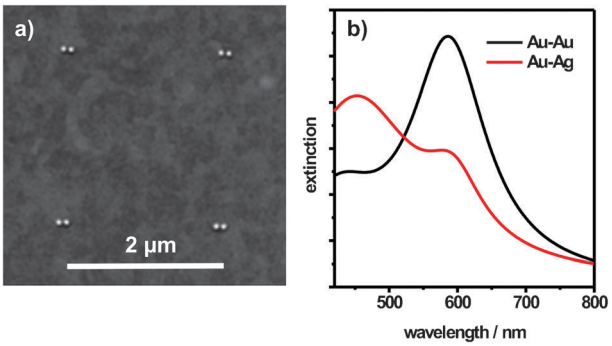

Fig. 1 (a) SEM image of Au–Ag dimer arrays fabricated on the ITO–glass substrate. (b) Extinction spectra of the Au–Au dimers and the Au–Ag dimers.

On the same sample, Au–Au homodimers were fabricated. Fig. 1a shows the distribution of the dimers on the substrate. The diameter of the Au or Ag nanoparticles is approximately 50 nm, the height is 50 nm and the distance between them in the dimer is about 30 nm. The dimer pairs are separated by approximately 2 μm to be able to measure the structures separately.

The optical properties of the Au dimer sample were measured on a home-built confocal optical microscope. This microscope uses a parabolic mirror (numerical aperture = 0.998) for laser focusing and signal collection, instead of an objective lens. The parabolic mirror is positioned above the sample and collects optical signals from an open angle of nearly 180° which is especially important for detecting weak optical signals. An ultra-short pulse laser (~100 fs, 770 nm, 90 MHz) is focused using the parabolic mirror by reflection onto its focal spot where the sample is positioned. A Gaussian polarized laser beam was used during the measurements and was polarized parallel to the dimer long axis. The blue-shifted optical signal was separated from the elastically scattered laser light using a short pass filter. The optical signal was either detected using a thermoelectrically cooled CCD-camera connected to a spectrometer (600 grating) or using a blue sensitive single photon detector (avalanche photodiode (APD)) for 2PPL and SHG imaging.

The optical images of the Au–Au homodimer array and the Au–Ag heterodimers are shown in Fig. 2a and b. The optical signals of the Au–Au dimers and of the Au–Ag dimers slightly vary throughout the samples. Some random intensity variation may be due to the minor shape and geometry variations of the lithographically fabricated nanoparticles. In general, the Au–Au dimers exhibit about four times stronger intensity than the Au–Ag dimers. Each optical pattern visualized in Fig. 2c has a full width half maximum (FWHM) around 270 nm. This is clearly below the Abbe limit that is 375 nm considering the polarisation conditions and the excitation wavelength. To understand such a phenomenon, a cross section through an optical pattern recorded from an Au–Au dimer is shown (squared black dots, Fig. 2c) as well as a linear measurement of a nanoparticle is shown for comparison (squared red dots). The black and the red curves are predicted from theoretical calculations.[20] These curves show the calculated intensity

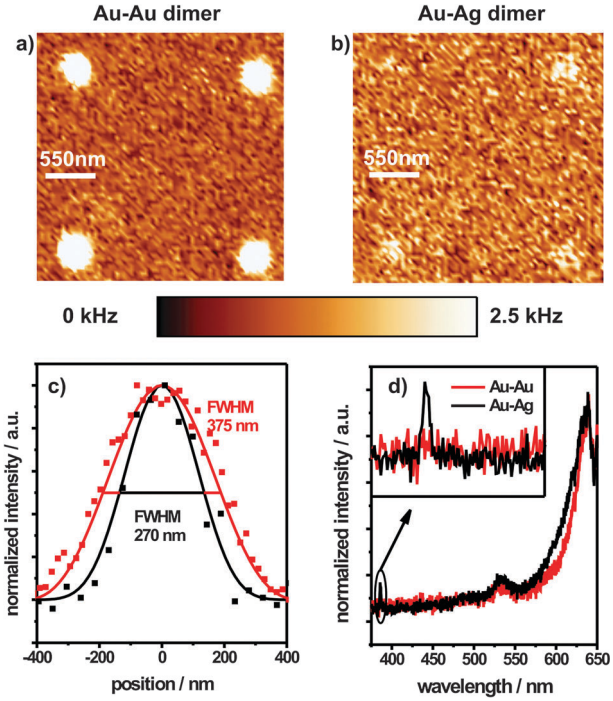

Fig. 2 Nonlinear optical imaging of (a) Au–Au dimer arrays and (b) Au–Ag dimer arrays. (c) The red curve shows a cross-section through the *xy*-*E*-field distribution in the focus of a linearly polarized Gaussian beam at an air/glass interface. The black curve shows a cross-section through the second power of the *xy*-*E*-field intensity distribution. The red and black squares indicate cross-sections through linear and non-linear optically imaged bright spots, respectively. (d) The black spectrum indicates the SHG and 2PPL signal from the Au–Ag dimers. The red spectrum shows the 2PPL signal from the Au–Au dimers.

distribution (E_{xy}^2, red) and the second power of the intensity distribution (E_{xy}^4, black) of a focused Gaussian polarized beam at the air/glass interface by a parabolic mirror. Due to the second-order non-linear effect, 2PPL and SHG signals show quadratic dependence on the impinging optical field. The cross-section of one experimentally measured bright Au–Au spot (squared black dots and black curve, Fig. 2c) exhibits clear agreement with the calculated E_{xy}^4 field distribution, indicating the typical second-order characteristics of the observed optical signal.

In Fig. 2d a spectral analysis of the signal obtained from Fig. 2a and b is shown. The ITO–glass substrate showed neither SHG nor 2PPL. Single particle measurements showed that the 2PPL of Au- and Ag-spectra look very similar. Both show a strong peak at around 640 nm and 530 nm. To compare the spectral shape the spectra taken from eight different dimers were averaged, the background was subtracted and the spectra were normalized. Two luminescence peaks are clearly seen for Au–Au dimers. They are at 637 and 532 nm, which are well known from transitions near the *X* and *L* symmetry points at the first Brillouin zone of crystalline Au.[21,22] In the two-photon excitation process, the relaxation of the electron–hole pair is either through nonradiative processes or by emission of luminescence. Besides the radiative channel through relaxation around the *X* and *L* points of the Brillouin zone, the

electron–hole pair can also couple with the LSP mode. When strong coupling between the excited electron–hole pair and the LSP happens, shaping of the 2PPL by the LSP profile can be observed.[23,24]

As seen from the extinction spectra (Fig. 1b), the Au–Au dimer shows a maximum extinction at around 586 nm; whilst the Au–Ag dimer has an extra extinction peak at about 453 nm. The excitation laser with a wavelength of 770 nm clearly falls in the extremely weak extinction range for both cases. Therefore, the excitation of collective electron motion of LSP mode in Au–Au and Au–Ag dimers is not efficient. Due to the inefficient excitation of the LSP in our experiments, the shaping of 2PPL by the LSP is not observable. Another possible reason might be the different substrates (ITO in our study *versus* glass or liquid in ref. 23 and 24). Further work is undergoing to clarify this question.

The energies of 2PPL depend on the particle (*e.g.* the aspect ratio and shape)[25] and can shift for several tens of nanometres. The 2PPL signal of the Au–Ag dimers looks very similar to that of the Au–Au dimers. However the peak seen at 639 nm broadens. This effect could be due to an extra broadband emission underneath the Au luminescence. For example, such a broadband emission ranging from 350 nm to 600 nm with a maximum between 500 nm and 550 nm was reported for nonlinear excited Ag before.[26–28] In addition, an Ag nanoparticle in an Au–Ag heterodimer has been reported to induce Fano profiles in the absorption spectrum of the Au nanoparticle since the localized SPR of the Ag nanoparticle can couple with the Au interband transitions.[29] Using a modified hybridization model including the interband absorption of Au, Sheikholeslami *et al.* have reported that the Ag LSPR mode was shifted in the Au–Ag dimer due to such a coupling effect, leading to a red-shifted interband continuum in the Au–Ag dimers compared to the case of individual nanoparticles. Further experiments are being carried out to investigate the contribution of such an effect in our system.

In the inset of Fig. 2d no SHG signal can be seen for the Au–Au dimers. In contrast, the Au–Ag dimers show a clear peak at 385 nm that can be assigned to the second harmonic of the laser wavelength. Both Au–Au and Au–Ag dimers give 2PPL; whilst only Au–Ag dimers produce the SHG signal. To understand such phenomena, we need to discuss the following issues. The probabilities for the SHG as well as 2PPL are closely related to the local electric field strength. In the case of field enhancement both effects are supposed to rise significantly. As reported by Jain *et al.*[30] decreasing the distance between two particles leads to coupling and a red shift of the dimer resonance. Heterodimers with smaller distances have also been reported before to lead to high field enhancement. Strong field enhancement was reported at around 3 nm particle spacing.[31] Slablab *et al.*[32] reported a SHG signal rise of 6 orders of magnitude resulting from approaching particles until they almost touched. However, in our case, excitation of both the Au–Au and Au–Ag dimers is at off-resonance conditions. Efficient resonance excitation of the dimers is unlikely. In addition, in our measurements the particles are separated by a distance of 30 nm, which is far from the close distance required for generating a high near-field. According to the trend predicted by the plasmon ruler equation defined by Jain *et al.*,[30] the gap distance of 30 nm leads to weak coupling of the dimer. Therefore, the confinement of near-field in the dimer alone is not enough to understand the above phenomenon. Additional factors such as the following have to be considered.

2PPL of Au relies on a two photon absorption process to produce an electron–hole pair. After scattering processes the excited state relaxes into a new energy state and recombines near the Fermi surface. This incoherent process involves a transition into a higher energy level and does not depend on the symmetry of the dimer. SHG is a three photon process where two photons are absorbed as well, but no excited states are involved. A non-linear polarization is generated by two photons within the sample leading to a coherent radiation of a photon with double energy. This energy conversion depends on material properties like nonlinear second order susceptibility and non-centrosymmetry. Recently Berthelot *et al.* reported that the SHG responses at strongly interacting optical gap antennas can be significantly suppressed. Coupling homodimers along their long axes retains the centrosymmetry of the system, preserving thus the nonradiative nature of the SHG antenna mode, leading to silencing of the SHG signal.[33] Such a silencing effect is more dramatic when stronger interaction occurs between the gap antenna. The invisibility of the SHG in the centrosymmetric Au–Au dimers is likely due to the same reason. However in the Au–Ag heterodimer, composition asymmetry breaks the centrosymmetry of the dimer configuration, giving rise to the SHG peak that is shown in Fig. 2d. The dimer's symmetry along the antenna axis is perturbed when the material of one of the particles is changed, and so the SHG signal originating from the dimer is expected to rise in this case.

In summary, we investigated the influences of compositional asymmetry on the 2PPL and SHG processes in weakly coupled Au–Au and Au–Ag dimers. The presence of an Ag nanoparticle in the Au–Ag heterodimer led to slightly broadened 2PPL near the *X* symmetry point at the first Brillouin zone of Au, whilst the *L* symmetry point stayed the same. In addition, the weakly coupled Au–Ag heterodimer generated a strong SHG peak that is invisible in the Au–Au homodimers, indicating the importance of compositional asymmetry in the SHG process of dimer configuration. Further investigations regarding the gap-distance influences on the non-linear optical behaviour of heterodimers are underway.

Acknowledgements

We thank the ultrafast nanooptics project from the DFG (SPP 1391) for funding. The authors acknowledge the technical support of the platform Nano'Mat (www.nanomat.eu), financed by the ''Ministère de l'enseignement supérieur et de la recherche'', the ''Conseil régional Champagne-Ardenne'', the ''FEDER funds'' and the ''Conseil général de l'Aube''.

Notes and references

1 B. Palash, A. Pascal and N. Lukas, *Nanotechnology*, 2007, **18**, 044017.
2 J. N. Anker, W. P. Hall, O. Lyandres, N. C. Shah, J. Zhao and R. P. Van Duyne, *Nat. Mater.*, 2008, **7**, 442–453.
3 J. Rodríguez-Fernández, A. M. Funston, J. Pérez-Juste, R. A. Álvarez-Puebla, L. M. Liz-Marzán and P. Mulvaney, *Phys. Chem. Chem. Phys.*, 2009, **11**, 5909–5914.
4 M. A. van Dijk, M. Lippitz and M. Orrit, *Acc. Chem. Res.*, 2005, **38**, 594–601.
5 Y. Fu, J. Zhang and J. R. Lakowicz, *J. Am. Chem. Soc.*, 2010, **132**, 5540–5541.
6 F. Wackenhut, A. V. Failla, T. Züchner, M. Steiner and A. J. Meixner, *Appl. Phys. Lett.*, 2012, **100**, 263102–263105.
7 J. Jiao, X. Wang, F. Wackenhut, A. Horneber, L. Chen, A. V. Failla, A. J. Meixner and D. Zhang, *ChemPhysChem*, 2012, **13**, 952–958.
8 D. P. Fromm, A. Sundaramurthy, P. J. Schuck, G. Kino and W. E. Moerner, *Nano Lett.*, 2004, **4**, 957–961.
9 M. Fleischer, C. Stanciu, F. Stade, J. Stadler, K. Braun, A. Heeren, M. Haffner, D. P. Kern and A. J. Meixner, *Appl. Phys. Lett.*, 2008, **93**, 111114.
10 P. Mühlschlegel, H.-J. Eisler, O. J. F. Martin, B. Hecht and D. W. Pohl, *Science*, 2005, **308**, 1607–1609.
11 T. Kosako, Y. Kadoya and H. F. Hofmann, *Nat. Photonics*, 2010, **4**, 312–315.
12 J. B. Lassiter, J. Aizpurua, L. I. Hernandez, D. W. Brandl, I. Romero, S. Lal, J. H. Hafner, P. Nordlander and N. J. Halas, *Nano Lett.*, 2008, **8**, 1212–1218.
13 C. E. Talley, J. B. Jackson, C. Oubre, N. K. Grady, C. W. Hollars, S. M. Lane, T. R. Huser, P. Nordlander and N. J. Halas, *Nano Lett.*, 2005, **5**, 1569–1574.
14 E. Prodan, C. Radloff, N. J. Halas and P. Nordlander, *Science*, 2003, **302**, 419–422.
15 S. Sheikholeslami, Y.-w. Jun, P. K. Jain and A. P. Alivisatos, *Nano Lett.*, 2010, **10**, 2655–2660.
16 K. D. Ko, A. Kumar, K. H. Fung, R. Ambekar, G. L. Liu, N. X. Fang and K. C. Toussaint, *Nano Lett.*, 2010, **11**, 61–65.
17 M. Danckwerts and L. Novotny, *Phys. Rev. Lett.*, 2007, **98**, 026104.
18 S. Palomba, M. Danckwerts and L. Novotny, *J. Opt. A: Pure Appl. Opt.*, 2009, **11**, 114030.
19 B. Lamprecht, A. Leitner and F. R. Aussenegg, *Appl. Phys. B: Lasers Opt.*, 1999, **68**, 419–423.
20 M. Lieb and A. Meixner, *Opt. Express*, 2001, **8**, 458–474.
21 M. R. Beversluis, A. Bouhelier and L. Novotny, *Phys. Rev. B: Condens. Matter Mater. Phys.*, 2003, **68**, 115433.
22 K. Imura, T. Nagahara and H. Okamoto, *J. Phys. Chem. B*, 2005, **109**, 13214–13220.
23 A. Bouhelier, R. Bachelot, G. Lerondel, S. Kostcheev, P. Royer and G. P. Wiederrecht, *Phys. Rev. Lett.*, 2005, **95**, 267405.
24 M. Loumaigne, P. Vasanthakumar, A. Richard and A. Debarre, *Phys. Chem. Chem. Phys.*, 2011, **13**, 11597–11605.
25 K. Imura and H. Okamoto, *J. Phys. Chem. B*, 2009, **113**, 11756–11759.
26 W. Gan, G. Gonella, M. Zhang and H. L. Dai, *J. Chem. Phys.*, 2011, **134**, 041104.
27 C. K. Chen, A. R. B. de Castro and Y. R. Shen, *Phys. Rev. Lett.*, 1981, **46**, 145–148.
28 N. J. Borys, M. J. Walter and J. M. Lupton, *Phys. Rev. B: Condens. Matter Mater. Phys.*, 2009, **80**, 161407.
29 G. Bachelier, I. Russier-Antoine, E. Benichou, C. Jonin, N. D. Fatti, F. Vallée and P. F. Brevet, *Phys. Rev. Lett.*, 2008, **101**, 197401.
30 P. K. Jain, W. Huang and M. A. El-Sayed, *Nano Lett.*, 2007, **7**, 2080–2088.
31 F. Y. Chen, N. Alemu and R. L. Johnston, *AIP Adv.*, 2011, **1**, 032134.
32 A. Slablab, L. Le Xuan, M. Zielinski, Y. de Wilde, V. Jacques, D. Chauvat and J. F. Roch, *Opt. Express*, 2012, **20**, 220–227.
33 J. Berthelot, G. Bachelier, M. Song, P. Rai, G. C. des Francs, A. Dereux and A. Bouhelier, *Opt. Express*, 2012, **20**, 10498–10508.

